

Merging variable stiffness fiber patterns on multi-shape robotic sheets

Medha Goyal^{*1}, Maggy Lambo^{*1}, Josh Bongard², and Rebecca Kramer-Bottiglio¹

Abstract—Shape morphing can be achieved using thin, planar sheets patterned with strain-limiting constraints to direct differential growth into desired shapes. Our previous work produced such shape-shifting sheets using an inflatable sheet with variable stiffness fibers placed in patterns optimized by a multi-objective evolutionary algorithm. With our pipeline, we generated two specialized fiber patterns $\{P_i, P_j\}$ to produce shapes $\{S_i, S_j\}$, which we then layered onto the same sheet. However, this layering approach had translation inefficiencies in hardware, such as fiber redundancies. To reduce fiber crowding and increase shape fidelity, we propose that fibers identified as similar in both P_i and P_j can be implemented as a single fiber belonging to both patterns. Extending our previous work, herein we implement a post-optimization fiber merging protocol. Applying the protocol to sheets patterned with fibers targeting two shape-pairs, cylinder/sphere and simple saddle/monkey saddle, we demonstrate that fiber merging reduces the total number of fibers on each sheet, thus reducing sheet bulk and weight. We further measure the error between the target shapes and actual hardware shapes: For the cylinder/sphere shape-pair, the error increases with merging implemented when compared to the original, unmerged fiber patterns. For the monkey saddle/simple saddle shape-pair, the error decreases for one or both shapes for all fiber mergers implemented. The results indicate that fiber merging is increasingly useful with increasing fiber pattern complexity as measured by fiber count. Therefore, fiber merging is a potentially useful strategy to simplify the complexity of fiber designs required for shape-matching.

I. INTRODUCTION

Soft robots that adapt their form (shape) on-demand would be able to function across multiple environments or task contexts [1]. For thin sheets, incompatible local strains due to in-plane expansion creates out-of-plane buckling, yielding local curvature changes that can collectively translate to global shape change. The inverse problem of designing local differential growth patterns on a thin sheet to achieve a target shape has been solved analytically [2]. Several works have demonstrated shape-shifting sheets using a variety of materials including cellulose-embedded hydrogels [3], dielectric elastomers [4], pneumatic silicone bilayers, [5] [6], liquid-infused ribbed sheets [7], and rubber sheet kirigami [8]. While some of these systems are reversible, most achieve only a fixed, singular shape-change per device. Sheets that can morph into multiple shapes have been demonstrated

in systems where actuating components are patterned onto inert substrates [4], [8], [9] or variable stiffness components are patterned on expanding substrates [10], [11]. However, in these sheets that can achieve multiple curvatures, the constraints are placed in intuitive positions, limiting their access to complex shapes.

The inverse design problem of patterning sheets with constraints able to produce multiple complex, non-intuitive shapes was tackled by Yang et al. [12]. Therein, inextensible patches (introduced by Kim et. al [13]) were patterned on a radially inflating pneumatic bilayer according to solutions found using a genetic algorithm, initiating pre-determined out-of-plane deformations to produce target shapes. While the patches could be adhered, removed, and re-adhered to switch between patterns and produce multiple shapes on the same sheet, they worked passively and could not be selectively activated. Therefore, the sheet could not produce different shapes without manual reconfiguration of the inextensible fiber patches.

To allow for reconfiguration without manual intervention, Yang et. al replaced the inert patches with variable stiffness fibers [10]. These fibers work via 1D layer jamming and contain strips of silicone with inextensible polyester inclusions that jam under negative pressure (vacuum). When jammed, the fibers increase in tensile stiffness by over $20\times$, allowing them to constrain bilayer expansion and produce out-of-plane curvatures. The jamming can be reversed by removing the vacuum, resulting in passive fibers that no longer constrain local growth. Yang et. al [10] used the variable stiffness fibers on the surface of an inflatable sheet to produce basic curvatures. We expanded on this by introducing a generalized simulation-to-reality (sim2real) pipeline that accepts two input shapes $\{S_i, S_j\}$ and generates two fiber patterns $\{P_i, P_j\}$, one for each shape, using a multi-objective evolutionary algorithm [14]. The two fiber patterns were overlaid to create a multi-shape sheet: shape S_i was accessed by stiffening P_i and slackening P_j , and shape S_j by slackening P_i and stiffening P_j . Designs for a sheet that could switch between cylindrical and spherical curvatures were successfully transferred into hardware in [14], demonstrating the feasibility of this pipeline.

The optimization algorithm used in our prior work returned designs consisting of fiber patterns for two target shapes on a single sheet. Each pattern was compared against its own corresponding target shape and errors for each shape were reported separately. Each combined design was regarded as a whole only when being checked for violations of hardware constraints, such as the presence of too many fibers or fibers that were too short to feasibly manufacture. In

*Authors contributed equally.

¹Department of Mechanical Engineering & Materials Science, Yale University, New Haven CT, USA. email: {medha.goyal, maggy.lambo, rebecca.kramer}@yale.edu

²Department of Computer Science, University of Vermont, Burlington VT, USA. email: jrbongard@uvm.edu

This material is based upon work supported by the National Science Foundation (NSF) under the Emerging Frontiers in Research and Innovation (EFRI) program (EFMA-1830870) and the Designing Materials to Revolutionize and Engineer our Future (DMREF) program (CMMI-2118988).

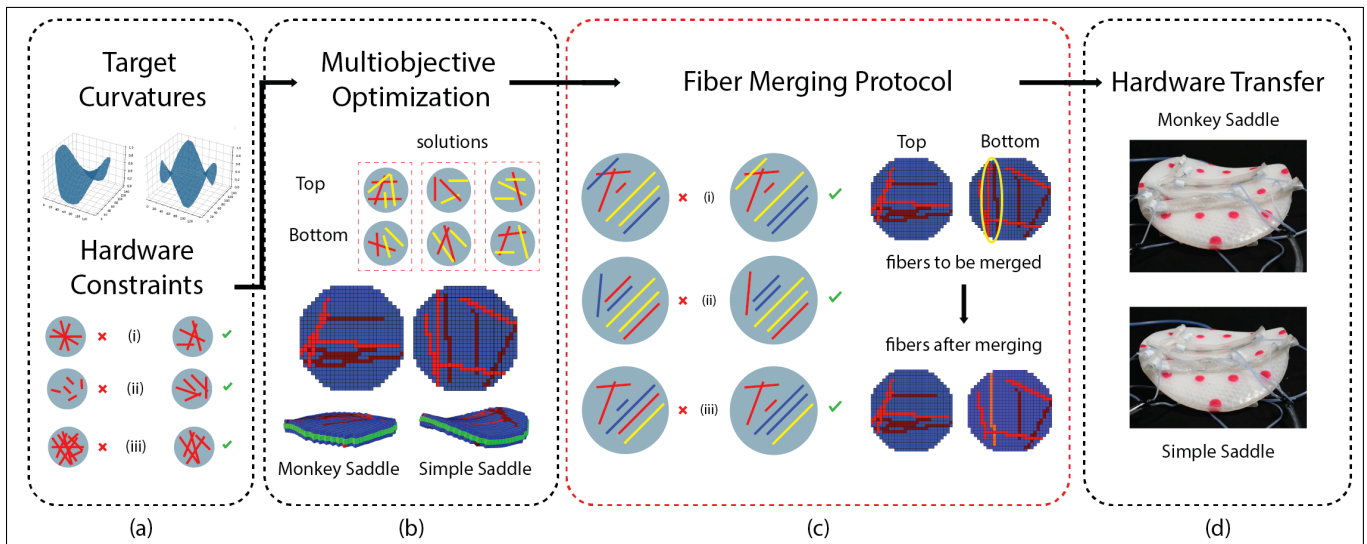


Fig. 1. **Pipeline overview.** (a): Two target curvatures (for example, simple saddle on the left and monkey saddle on the right) and constraints imposed by the hardware. Constraints are too many intersecting fibers (a-i), overly short fibers (a-ii), and too many fibers (a-iii). (b): An evolutionary multi-objective optimization algorithm finds a set of solutions that satisfy the objectives to varying degrees. Each solution set has a pattern of fibers (shown as red and yellow) on the top and bottom of the sheet. Red fibers correlate to the first target shape; yellow fibers correlate to the second target shape. Simulated inflations with each shape-pattern activated (now shown as bright and dark red) yield shape-matching to each target shape. (c): The fiber merging protocol is applied post-optimization. Candidate fibers to merge must be in close proximity, defined as less than half of the sheet diameter (c-i); have a similar orientation, defined as being less than 10° off parallel (c-ii); and be similar in length, with less than 2 cm variation (c-iii). The fiber pair must also comprise one fiber from each pattern associated with the target shapes. Merging is performed on the chosen fiber patterns to simplify the designs. (d): The original and merged designs are transferred to hardware.

disregarding the presence and impact of one fiber pattern on the other— P_i still passively exists while inactive, and therefore affects the shape fidelity of S_j when P_j is active—the prior sim2real pipeline misses the opportunity to consider the shape similarity between the two target shapes programmed onto the same sheet and leverage this similarity to simplify the resulting overlaid fiber patterns.

Shape similarity between two target shapes may imply fiber redundancies, or two fibers that belong to the unique patterns P_i and P_j but are close together and “crowded.” To exploit shape similarity, reduce fiber crowding, and potentially increase shape fidelity, we propose that fibers identified as similar in both P_i and P_j can be implemented as a single fiber belonging to both patterns. Merging a pair of fibers reduces the total fiber count in the set $\{P_i, P_j\}$ by one.

A lower fiber count is desirable for a few reasons. First, the simulation models fibers as being embedded into the sheet instead of sitting atop the sheet, as is the case in reality. Therefore, each additional fiber adds weight and bulk not accounted for in the model, introducing a source of error. Second, reducing the number of fibers reduces the labor required for fabrication, speeding up the sim2real transfer. Third, using fewer fibers frees up space on the sheet, which could allow the transfer of more complex target shapes or potentially even a third curvature.

Our work tackles this problem by exploring how fibers associated with one target shape might aid in producing the other shape. We consider designs for the multi-shape shifting sheets found in simulation in our prior work [14], looking for similarities between the fiber patterns associated with each

shape. For a shape-pair $\{S_i, S_j\}$, we layer the unique fiber patterns $\{P_i, P_j\}$ generated by evolutionary optimization and implement a post-optimization fiber merging protocol (Fig. 1). We identify fiber pairs, where one fiber is from P_i and one is from P_j , and choose pairs that appear to constrain the sheet in similar ways when producing the target shapes.

Whereas fiber patterns found previously contained fibers that would only be active (jammed) for one shape or the other, by implementing fiber merging, we replace some pairs of fibers with a single fiber that is active (jammed) for both shapes. This fiber merging strategy reduces the total number of fibers required on the sheet for multi-shape access. We show visually and by sampling inflation values across representative points that for simple shapes requiring fewer fibers (cylinder/sphere curvatures), reducing the number of fibers causes the shape to diverge from the target shapes. For more complex target shape-pairs (simple saddle/monkey saddle) consisting of more total fibers, implementing one fiber merger has a negligible effect on shape fidelity, and implementing a second fiber merger slightly improves the monkey saddle (while slightly worsening the simple saddle).

Overall, the results herein demonstrate that fiber patterns including fiber mergers have the potential to match at least two target shapes with a similar target-to-real error as the original patterns (without fiber mergers) while requiring fewer fibers. The results thus suggest that the introduction of post-optimization fiber merging is a useful strategy to decrease the fiber count while increasing the shape fidelity of some shapes, and the strategy’s efficacy is dependent on fiber count and similarities between the target shapes.

II. METHODS

A. Fiber Designs: Original

Two fiber patterns from our prior work [14] were transferred into hardware: one for a sheet that switches between cylindrical and spherical curvatures, the other for a sheet that switches between monkey saddle and simple saddle curvatures. Among the cylinder/sphere designs presented in [14], all had the same number of fibers—six in total—and we selected “Design 3” from [14] (Fig. 2a,b) for its relatively low sim2real errors. Among the monkey saddle/simple saddle designs, we again selected “Design 3” from [14] (Fig. 2c,d) for its lower number of fibers—14 in total—relative to the other designs.

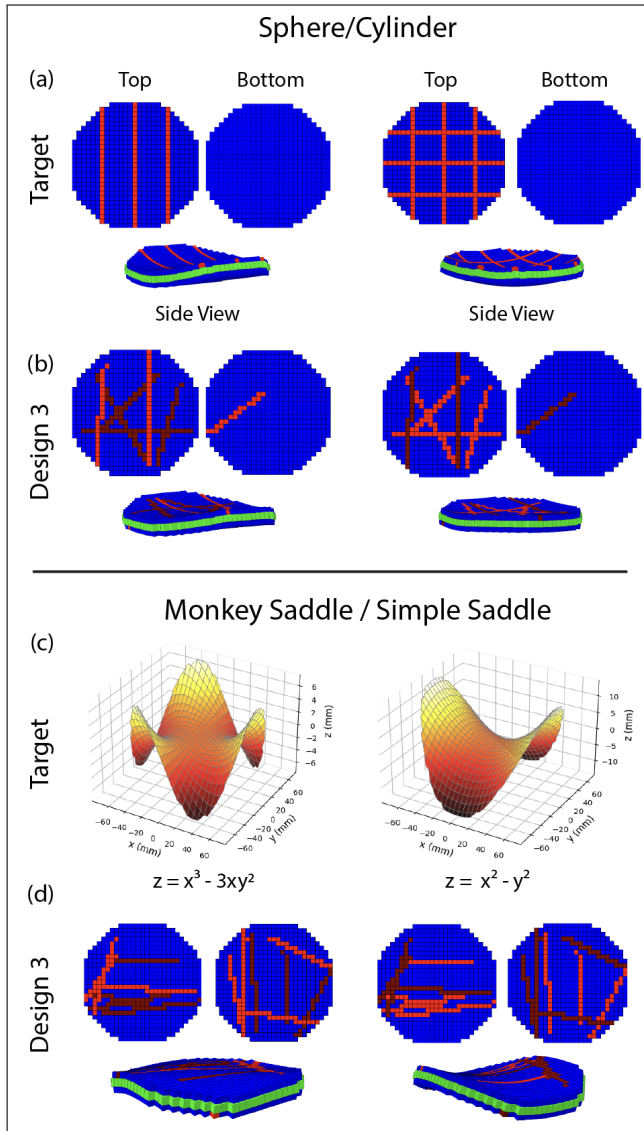


Fig. 2. Target shapes and simulated designs chosen for hardware implementation. (a, c) The target shapes for (a) the cylinder and sphere shape-pair, and (c) the monkey saddle and simple saddle shape-pair. (b, d) The fiber pattern designs for (b) cylinder and sphere, and (d) monkey saddle and simple saddle, found by the multi-objective algorithm [14] and chosen for our study. Adapted with permission [14]. Copyright 2023, IEEE.

B. Fiber Designs: Requirements for Merging

Merged patterns were created by identifying pairs of fibers across designs that appeared to serve the same function as one another. Although line clustering algorithms exist [15], the current work aims to investigate nonlinear interactions when fibers are close to or pass over one another, which are unique challenges. Therefore, in this work, fiber mergers were achieved by ensuring each fiber pair satisfied a set of conditions described as follows: a) each fiber pair contains one fiber from subset P_i and one fiber from subset P_j ; b) the fibers have a similar orientation, defined as being less than 10° off parallel; c) the fibers are similar in length with less than 2 cm variation; and d) the fibers are in close proximity, defined as less than half of the sheet diameter. These conditions were chosen because they describe the smallest separation between any two fiber pairs as observed by the eye for the designs explored in this paper. Each pair that satisfied these conditions was merged by being replaced with a single fiber placed at their midpoint in the same orientation and with a length equal to their average, described in more detail in Section II-D.

C. Transferring Designs to Hardware

Each shape-shifting sheet consists of a flat, circular, pneumatically driven bladder made of Ecoflex 50, containing a uniform grid of pillars that limit expansion in the z -direction, patterned with variable stiffness fibers as described in prior works [10], [14]. Each fiber contains strips of Ecoflex-50 (Smooth-On) with polyester thread inclusions. The strips slide past one another at atmospheric pressure but are jammed into contact under vacuum, creating a force chain that amplifies the fiber’s tensile strain by over $20\times$ and constrains the sheet’s expansion along its length, producing out-of-plane deformation when the sheet expands. Fibers were adhered to the sheet using Silpoxy™ (Smooth-On).

Variable stiffness fibers were fabricated with lengths and placements according to designs chosen from the multi-objective algorithm in our previous work [14], as described in Section II-B. The fibers were jammed with vacuum to activate a target shape. The sheets were inflated and held at 5.0 ± 0.1 psi for both cylinder/sphere sheets and at 4.0 ± 0.1 psi for all saddle/monkey saddle sheets. The inflation pressures were chosen to ensure that the curvature was visible by the eye but not so high that the sheets were strained close to the point of rupture.

D. Design of Experiments

In our prior work, we searched for two variable stiffness fiber patterns P_i and P_j , which were overlaid onto one sheet, enabling us to switch between two shapes S_i and S_j . In this work, we find pairs of fibers such that one fiber is part of P_i and the other fiber is part of P_j . We measure the distance between each pair of fibers d , the length of each fiber l_i and l_j , and the angle of one fiber with respect to the other, α . For all $\alpha < 10^\circ$, d less than half the sheet diameter, and $|l_i - l_j| < 2$, the pair of fibers is replaced with a single representative fiber of length $(l_i + l_j)/2$ at an angle of $\alpha/2$

with respect to one of the original fibers, and at the midpoint between the positions of the two original fibers (a distance of $d/2$ between the two original placements).

Following these thresholds and guidelines for fiber merging, we ask: Does merging two fibers—one each from P_i and P_j , into a single fiber belonging to both $\{P_i, P_j\}$ —affect the shape fidelity of S_i and S_j ? We answer this question by measuring the error between the target shapes and the real inflated shapes S_i and S_j . We did this for two sets of shape pairs: $\{P_i, P_j\} = \{\text{cylinder, sphere}\}$ and $\{\text{monkey saddle, simple saddle}\}$.

E. Error Calculation

To compare the error between hardware curvatures and target curvatures, we measured the z coordinates of 15-16 representative points and compared them to the z coordinates at the corresponding x - and y - positions of the target

curvature with the following equation:

$$e = \frac{\sum_{i=1}^{n_p} |r_i - s_i|}{n_p} \quad (1)$$

where e is the target-to-hardware error, r_i is the z -coordinate (height) of the sheet at point i in hardware (normalized by the greatest height difference), s_i is the normalized height of the target curvature, and n_p is the number of points measured.

III. RESULTS & DISCUSSION

Applying the merging rules listed in Section II-D to the fiber patterns chosen from [14] yielded one candidate fiber pair for merging in the cylinder/sphere design (Fig. 3a) and two candidate fiber pairs (which we will call fiber pairs A and B) in the simple saddle/monkey saddle design (Fig. 3b,c). The following six fiber patterns were subsequently transferred into hardware: (1) the original design without merging for cylinder/sphere, (2) a design with one merge in cylinder/sphere, (3) the original design without merging for simple saddle/monkey saddle, (4) a design with fiber pair A merged in simple saddle/monkey saddle, (5) a design with fiber pair B merged in simple saddle/monkey saddle, and (6) a design with both fiber pairs A and B merged in simple saddle/monkey saddle (Fig. 3d).

We assessed the error between the original designs and merged designs by comparing the curvature produced in hardware for each shape to the target curvature (defined mathematically). Images of hardware inflation of the sphere and cylinder shapes are shown in Fig. 4, and the simple saddle and monkey saddle are shown in Fig. 5. The quantitative error results are given in Tables I and II.

The results indicate that for the cylinder/sphere design, merging a pair of fibers into a single fiber that belongs to both shape patterns yields inflated shapes that are less faithful to the target shapes, compared to those produced by the

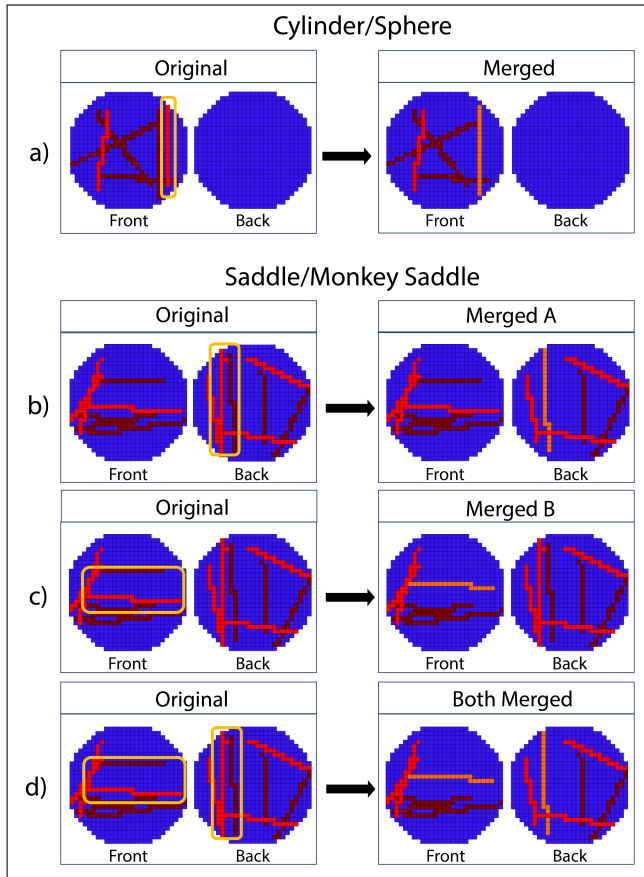


Fig. 3. **Fiber pairs selected for merging.** Original, unmerged designs found in simulation [14] are shown on the left. Pairs of fibers identified as candidates for merging are circled in yellow. The subsequent merged designs are shown on the right. (a) Original (left) and merged (right) fiber designs for cylinder/sphere. The subset of fibers shown in bright red corresponds to the cylinder curvature; dark red fibers correspond to the sphere curvature. (b) The original design for simple saddle/monkey saddle with merge pair A circled (left), and Merge A implemented (right). Bright red fibers correspond to the monkey saddle curvature; dark red fibers correspond to the simple saddle curvature. (c) The original design for simple saddle/monkey saddle with merge pair B circled (left), and Merge B implemented (right). (d) The original design for simple saddle/monkey saddle with merge pairs A and B circled (left), and both merges implemented (right).

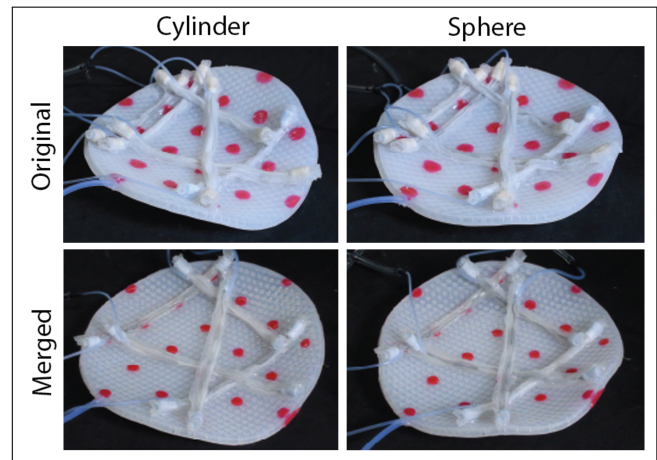


Fig. 4. **Cylinder and sphere sheet inflations in hardware.** Original and merged designs were transferred to hardware. Shapes were attained by activating the subset of fibers corresponding to each target shape during sheet inflation. The merged fiber patterns visually contain one less fiber than their unmerged fiber pattern counterparts. Sheet diameter = 14 cm.

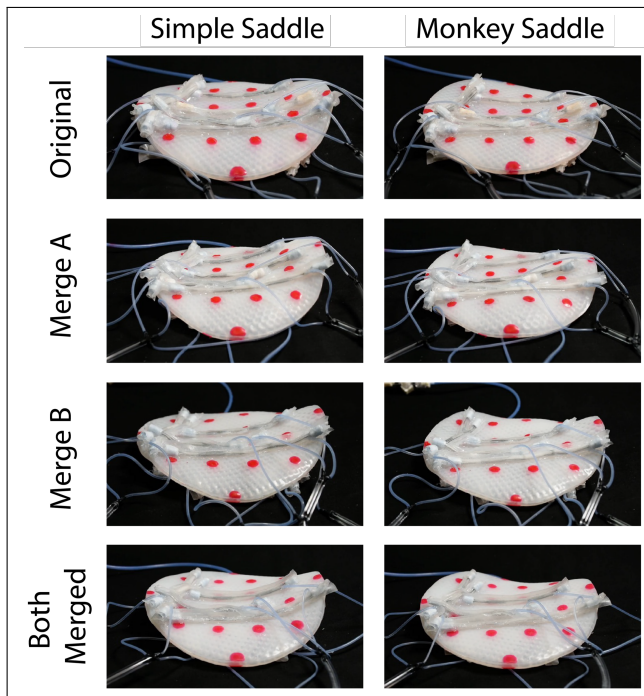


Fig. 5. Simple saddle and monkey saddle sheet inflations in hardware. Original and merged designs were transferred to hardware. The resulting inflations are shown for each sheet (original, Merge A, Merge B, and both merged), where the subset of fibers corresponding to each target shape was selectively activated, producing either a simple saddle or monkey saddle. Sheet diameter = 14 cm.

TABLE I
ERROR BETWEEN HARDWARE & TARGET CURVATURES:
CYLINDER/SPHERE

Sheet	Cylinder e	Sphere e
Original	10.7% \pm 1.6%	10.0% \pm 0.9%
Merged	31.2% \pm 1.5%	36.7% \pm 2.2%

TABLE II
ERROR BETWEEN HARDWARE & TARGET CURVATURES: SIMPLE
SADDLE/MONKEY SADDLE

Sheet	Simple Saddle e	Monkey Saddle e
Original	15.4% \pm 1.4%	20.5% \pm 0.5%
Merge A	12.2% \pm 0.5%	20.3% \pm 0.8%
Merge B	14.8% \pm 1.5%	23.7% \pm 1.0%
Both Merged	19.2% \pm 1.0%	18.6% \pm 0.5%

original, unmerged fiber patterns. The increased error e is seen for both the cylinder and the sphere shapes.

For the simple saddle/monkey saddle designs, we implement two fiber pair mergers, which we denote as Merge A and Merge B. Merge A slightly improves the shape fidelity of the simple saddle shape and has a negligible effect on the monkey saddle. Merge B has a negligible effect on the simple saddle shape and slightly worsens the shape fidelity of the monkey saddle. Implementing both merges slightly worsens the simple saddle while improving the monkey saddle shape.

We surmise that merging was a disadvantageous strategy for the simpler cylinder/sphere shapes due to their low number of fibers: six for the unmerged pattern, which was

reduced to five for the merged pattern. With fewer total fibers, each fiber on average contributes more to the system's shape. Therefore, the absence of even one fiber could substantially impact shape fidelity.

In contrast, the errors for the sheets patterned for simple saddle/monkey saddle shapes were not substantially impacted by a single pair of fibers merging, regardless of which pair was merged. The monkey saddle error notably decreased after two fiber pair merges. We speculate that because the simple saddle/monkey saddle design has a relatively greater number of fibers (14 total fibers), the presence of more fibers adds weight and bulk to the sheet. With two fibers eliminated via merging (12 total fibers when both pairs A and B are merged), some weight is removed allowing the sheet to inflate in a manner more similar to the target shape. Our visual inspections support this suggestion: an asymmetry was observed during inflation for the simple saddle/monkey saddle sheets, where the side of the sheet with a greater concentration of fibers (the left in Fig. 5), had a less pronounced inflation than the other side.

IV. CONCLUSION AND FUTURE WORK

Our prior works introduced variable stiffness fibers that can be patterned on inflatable sheets to selectively constrain inflation and produce designed inflated shapes. We proposed a sim2real pipeline to generate (using a multi-objective evolutionary algorithm) unique fiber patterns for target shapes, which could be overlaid to achieve a multi-shape sheet [14]. Activating one unique pattern would produce one shape, and activating the other unique pattern would produce the other shape. However, we found that overlaying unique patterns caused fiber crowding on the sheet—a problem that would become increasingly severe with an increasing number of target sheet shapes. To alleviate this problem, we implemented a strategy to merge redundant fibers.

In general, fiber patterns may be more easily merged if they are similar, where a fiber identified as similar in both fiber patterns P_i and P_j can be implemented as a single fiber belonging to both patterns to reduce crowding. We proposed a set of thresholds to identify pairs of candidate fibers, where each fiber of the pair belongs to a different fiber pattern (and is associated with a different target shape). For the mergeable fiber pairs, we replaced each pair with a single representative fiber of averaged length at the midpoint of their separation by both distance and angle.

We explored the viability of this merging strategy as a post-processing step for further simplifying designs found in simulation on two target shape-pairs: 1) cylinder/sphere and 2) simple saddle/monkey-saddle. We selected one design produced in simulation for each case, applied merging rules to the designs, replicated the original designs and merged designs in hardware, and compared the shapes produced before and after merging. We demonstrated that all fiber patterns, original and merged, successfully produced the target shapes with reasonable fidelity and errors comparable to those previously reported.

By comparing the shapes produced by our original and merged designs to the target shapes, we observed that merging increases the target-to-hardware error in sheets with fewer fibers, but can improve or negligibly affect shape matching for sheets with more complex features that require a greater number of fibers. This finding suggests that fiber merging is a useful strategy to simplify complex fiber patterns, reducing both the labor required to transfer designs to hardware and the bulk that could be weighing the sheet down and potentially contributing to the error. Future work will investigate the variables associated with pattern complexity (e.g., fiber count, number of fiber intersections) to elucidate the thresholds at which merging becomes advantageous.

Since we only compared multiple inflations of a single sample in this work, future work should consider sample variance. Further insight into the efficacy of fiber merging for pattern simplification and shape-fidelity enhancement could also be gleaned in simulation, where errors between target and simulated shapes could be assessed much faster than target-to-hardware errors.

In this work, we studied the impacts of merging as applied to fiber pairs that were aligned in orientation, similar in length, and in proximity to one another relative to other fiber pairs. Future work could explore these variables further and determine the extent to which merging is useful for fiber pairs of different lengths, relative angles, and separation distances, and whether additional merging steps are beneficial. Opening up the parameter space could give us more options for merging when fiber patterns are found via simulation and optimization, and also a tool to empirically investigate which fibers contribute the most to producing a target shape, to guide the choice of candidates for merging.

Herein, we focused on relatively related shape pairs, as we aimed to exploit their shape similarities. Future work could instead utilize pairs of dissimilar target shapes not typically placed on the same sheet, such as cylinder and monkey saddle. The study of multi-shape sheets capable of switching between two relatively dissimilar shapes may elucidate quantitative metrics to evaluate shape similarity in the context of fiber merging. Furthermore, such metrics may reveal thresholds corresponding to the likelihood that a shape-pair will contain mergeable fibers.

As merging rules are simultaneously expanded and refined (i.e., the design space gets larger while we systematically narrow the candidate fiber pairs), merging could be integrated into the simulation and optimization components of our pipeline. For instance, a neural network could learn latent representations of fiber patterns for various shapes. Additional training could then be performed to ensure that decompressing linear combinations of latent representations drawn from different shapes results in appropriately merged fiber patterns. In the longer term, artificial intelligence (AI) models that successfully generate images from text prompts may be adapted to generate fiber patterns from text prompts that describe individual target shapes, resulting in a trained generative model that generates merged fiber patterns from text prompts that describe a set of different target shapes.

REFERENCES

- [1] D. Shah, B. Yang, S. Kriegman, M. Levin, J. Bongard, and R. Kramer-Bottiglio, "Shape changing robots: bioinspiration, simulation, and physical realization," *Advanced Materials*, vol. 33, no. 19, p. 2002882, 2021.
- [2] W. M. van Rees, E. Vouga, and L. Mahadevan, "Growth patterns for shape-shifting elastic bilayers," *Proceedings of the National Academy of Sciences*, vol. 114, p. 11597–11602, 2017.
- [3] A. Sydney Gladman, E. A. Matsumoto, R. G. Nuzzo, L. Mahadevan, and J. A. Lewis, "Biomimetic 4d printing," *Nature Materials*, vol. 15, no. 4, pp. 413–418, 2016.
- [4] E. Hajiesmaili, N. M. Larson, J. A. Lewis, and D. R. Clarke, "Programmed shape-morphing into complex target shapes using architected dielectric elastomer actuators," *Science Advances*, vol. 8, no. 28, p. eabn9198, 2022.
- [5] J. Pikul, S. Li, H. Bai, R. Hanlon, I. Cohen, and R. F. Shepherd, "Stretchable surfaces with programmable 3d texture morphing for synthetic camouflage skins," *Science*, vol. 358, no. 6360, pp. 210–214, 2017.
- [6] E. Siéfert, E. Reyssat, J. Bico, and B. Roman, "Bio-inspired pneumatic shape-morphing elastomers," *Nature Materials*, vol. 18, no. 1, pp. 24–28, 2019.
- [7] J. Capello, B. Scheid, F. Brau, and E. Siefert, "Bioinspired shape shifting of liquid-infused rubber sheets," *PNAS*, vol. 120, no. 1, 2022.
- [8] G. P. Choi, L. H. Dudte, and L. Mahadevan, "Programming shape using kirigami tessellations," *Nature Materials*, vol. 18, no. 1, pp. 999–1004, 2019.
- [9] Y. Bai, H. Wang, Y. Xue, Y. Pan, J.-T. Kim, X. Ni, T.-L. Liu, Y. Yang, M. Han, Y. Huang *et al.*, "A dynamically reprogrammable surface with self-evolving shape morphing," *Nature*, vol. 609, no. 7928, pp. 701–708, 2022.
- [10] B. Yang, R. Baines, D. Shah, S. Patiballa, E. Thomas, M. Venkadesan, and R. Kramer-Bottiglio, "Reprogrammable soft actuation and shape-shifting via tensile jamming," *Science Advances*, vol. 7, no. 40, p. eabh2073, 2021.
- [11] R. Chellattoan and G. Lubineau, "A stretchable fiber with tunable stiffness for programmable shape change of soft robots," *Soft Robotics*, vol. 9, no. 6, pp. 1052–1061, 2022.
- [12] B. Yang, J. Powers, A. Parsa, J. Bongard, and R. Kramer-Bottiglio, "Shape matching: Evolving fiber constraints on a pneumatic bilayer," in *2021 IEEE 4th International Conference on Soft Robotics (RoboSoft)*. IEEE, 2021, pp. 630–635.
- [13] S. Y. Kim, R. Baines, J. Booth, N. Vasios, K. Bertoldi, and R. Kramer-Bottiglio, "Reconfigurable soft body trajectories using unidirectionally stretchable composite laminae," *Nature Communications*, vol. 10, no. 1, p. 3464, 2019.
- [14] A. Parsa, M. Goyal, M. Lambo, B. Yang, B. Josh, and R. Kramer-Bottiglio, "Evolving variable stiffness fiber patterns for multi-shape robotic sheets," in *2023 IEEE International 6th International Conference on Soft Robotics (RoboSoft)*. IEEE, 2023, pp. 1–7.
- [15] J. C. R. Thomas, "A new clustering algorithm based on k-means using a line segment as prototype," pp. 638–645, 2011.